https://doi.org/10.15255/KUI.2021.073
KUI-33/2022
Original scientific paper
Received November 13, 2021
Accepted March 17, 2022

Study of Spraying Technology on Absorber Performances in a H_2O/LiBr Absorption Chiller

W. Maouche,[a*] *M. Douani*,[a] *A. Labbaci*,[b] *Ü. Tezcan Ün*,[c] and *M. Derakhshandeh*[d]

[a] Processes Engineering Department, University of Hassiba Benbouali Chlef, Green Chemistry-Water-Energy Laboratory, B.P. 151, Chlef 02 000, Algeria
[b] Processes Engineering Department, Water and Environment Laboratory, University of Hassiba Benbouali, B.P. 151, Chlef 02 000, Algeria
[c] Department of Environmental Engineering, Eskisehir Technical University, 26 555 Eskisehir, Turkey
[d] Engineering Faculty, Life Science and Biomedical Engineering Application and Research Center, Istanbul Gelisim University, 34 310 Istanbul, Turkey

Abstract

For major thermal engines used in industrial sectors, the use of chillers has been growing steadily over the previous decades. Indeed, this is linked strongly to their large energy performance despite their investment costs, which are still high, in particular for low powers. Performance coefficients for absorption chillers are relatively low, and their profitability depends on the costs of the main equipment and more particularly on the price of the absorber. Several studies focusing on the development of mass contactors are underway with the principal objective of further improving their performance of mass and energy transfer. Relating to the mass and heat transfer, it is specified that the contact between the phases in circulation is ensured by different types of contactors. The transfer performance is correlated with the heat and mass transfer coefficient on the one hand, and the specific exchange area, *i.e.,* the exchange area *per* unit volume of the contactor on the other hand. These contactors are distinguished by their mode of contact between phases (bubbling, spraying, falling film, *etc.*). While the exchange coefficient depends on the hydrodynamics regime in the contactor (flow regime and physicochemical properties of phases), the specific exchange area is dictated by its operating mode. Any limitation of its use for a specific application (physicochemical phenomena, such as crystallisation, deposited dust, *etc.*) requires research and development of better devices more adapted. Moreover, the most used contactors in chemical engineering are plate columns, packed columns, falling film columns, spray columns, *etc.* In order to intensify exchanges, a new absorber of the pulverised type is to be explored in relation with the physicochemical properties of the phases, and of their hydrodynamic flow conditions in the sprayed column. Therefore, an experimental study of the influence of operating variables (nozzle diameter, fluids flow rate, their concentrations, size of droplets, *etc.*) on the overall coefficient of mass transfer in gaseous phase in the absorber of the absorber chiller was conducted. After having fixed the pressure in the absorber, the first part of the study allowed developing new correlations linking the experimental results of the $K_G \cdot a$ to all operating variables ($\dot{L}$, $\dot{G}$, d_d, *etc.*). The second part was devoted to the simulation of the absorption chiller functioning by introducing the concept of energy and exergy yields based on the mass transfer correlations.

Keywords

H_2O/LiBr binary system, liquid vapour equilibrium, hydrodynamics of the spray absorber, overall coefficient of mass transfer, modelling

1 Introduction

Spray towers are used for gas absorption and stripping in many applications, including the removal of CO_2, SO_2, NO_x, and HCl from flue gases emitted by furnaces and incinerators using sprayed alkaline solutions.[1] The absorption of NH_3 from water spray and desorption of NH_3 from wastewater by air stripping is a common process.[2]

From an environmental point of view, the climate change and the preservation of natural resources require the implementation of a new energy transition policy.[3] In view of their operating flexibility, the absorption chillers present the best alternative to conventional compression machines, since on the one hand, they guarantee[4] a high efficiency for low thermal levels, and on the other hand, they are characterised by their low consumption of energy with lower maintenance cost viewing their robustness.[5]

Moreover, the absorption machines used in air conditioning systems allow significant savings in electrical consumption compared to traditional mechanical compression machines.[6] Thus, international community has set itself the goal of halving greenhouse gas emissions by 2050 on a global scale. To analyse the absorption chiller (A.C.) profitability, the concept of the coefficient of performance (COP) was often introduced. Indeed, for an A.C. presenting a good alternative, it was noted that its value varied in the range $0.2 < \mathrm{COP} < 0.37$.[7,8]

It essentially consists of four components: 1) condenser, 2) evaporator, 3) generator, and 4) absorber.[3]

* Corresponding author: Wahiba Maouche
Email: w.maouche@univ-chlef.dz

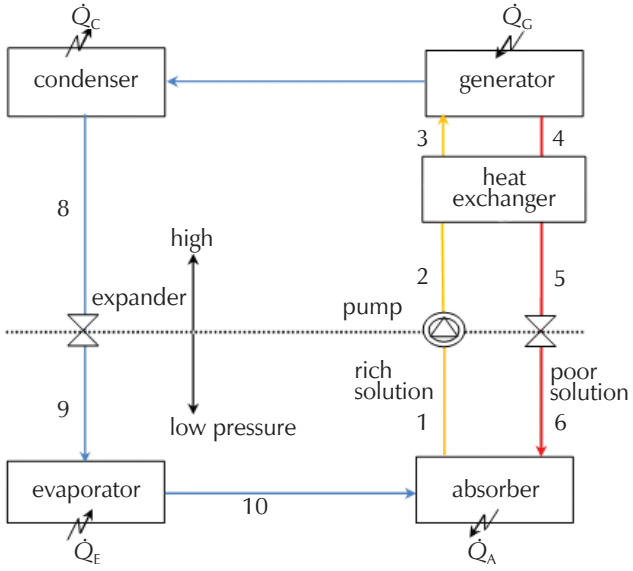

Fig. 1 – Technological diagram of an absorption chiller[9]

Strictly speaking, its functioning principle is based on the judicious choice of working couples, which is dictated by their thermodynamic behaviour and their ecological impact. It can be assimilated to a compression heat pump where both elements (generator and absorber) are replaced by the compressor; that is thermochemical compression. In its cooling mode and operating with water/LiBr as working couple, the rich stream and the poor stream in solvent circulate between the generator and the absorber (Fig. 1).[9]

In the absorber, the absorption of water vapour is accompanied by the release of thermal power, $\dot{Q}_A$ (W). That is the heat pump effect. At the generator, the rich solution is released from its water content following a bringing of power, $\dot{Q}_G$ (W). However, a devesiculator must be placed upstream of this element to trap any particles of LiBr that could be entrained by the water vapour stream. The water vapour is driven towards the condenser, where a power, $\dot{Q}_C$ (W), would be exchanged with the external medium.[10]

1.1 Theoretical aspects of the transfer

By neglecting the variation of kinetic and potential energies in the unit, the energy balance on the absorption chiller, exchanging heat, mass and shaft work with the external environment, can be written:

$$\dot{Q}_E + \dot{Q}_G - \dot{Q}_A - \dot{Q}_C + \dot{W}_p = \frac{dQ}{dt} \quad (1)$$

This expression of the energy balance on the control volume delimiting our absorption chiller is the subject of this study. It consists of the following parameters:

$\dot{Q}_E$ – flow rate of heat exchanged from the evaporator: this is the frigorific effect. Unit: W (energy/time).

$\dot{Q}_G$ – heat flow rate necessary for operation of the generator. Unit: W (energy/time).

$\dot{Q}_A$ – measuring of the heat flow rate exchanged at the absorber. Unit: W (energy/time).

$\dot{Q}_C$ – measuring of the heat flow rate exchanged at the condenser. Unit: W (energy/time).

$\dot{W}_p$ – shaft work applied with the external medium like power for a pump. Unit: W (energy/time).

d/dt(Q) – rate of energy increase (Q) inside the control volume by unit of time. This differential expression has the power unit.

In the Eq. (1), different signs take into account the universal thermodynamic convention of energy exchange: + means received by the control volume and − means lost from the control volume.

In steady state, the dynamic term, dQ/dt, is zero. Theoretically, the coefficient of performance (COP) is defined by:

$$\mathrm{COP} = \frac{\text{cooling capacity at the evaporater}}{\text{rate of heat input at the generator}} = \frac{\dot{Q}_E}{\dot{Q}_G + \dot{W}_p} \quad (2)$$

Generally, the pump energy is negligible compared to the thermal separation energy supplied to the generator. The expression of COP is reduced to:

$$\mathrm{COP} \cong \frac{\dot{Q}_E}{\dot{Q}_G} \quad (3)$$

It emerges that any increase in COP depends on the reduction of regeneration energy cost by the use of renewable energies (solar, warm utilities, *etc.*) on the one hand, and the increase in the power cleared at the evaporator, $\dot{Q}_E$, on the other hand. Taking into account the hypothesis of full evaporation of the stream from the condenser, it is clear that the flow rate of the stream leaving the evaporator, $\dot{L}_{10}$ would be exactly equal to the flow rate of the stream entering it, $\dot{L}_9$. Therefore, for a full evaporation, the mass and heat balances on the evaporator result in[11]:

$$\dot{L}_9 = \dot{L}_{10} \quad (4)$$

$$\dot{Q}_E = \dot{L}_{10} \cdot H_L^{T_E} \quad (5)$$

where $H_L^{T_E}$ is the latent heat of vaporisation of the condensate at the operating temperature of the evaporator, expressed in kJ kg^{-1}.

When the operating temperatures at the condenser and at the evaporator are supposedly fixed, then $\dot{Q}_E$ is mainly dependent on the condensate flow rate $\dot{L}_{10}$, which is strictly equal to the quantity of water absorbed; hence, the interest of intensifying the mass transfer in the absorber by the development of extended contact surface between phases. Several works are being carried out by refrigeration energy specialists to design new, more efficient absorbers.[12] Technically, various absorber configurations are mentioned in the literature[13]. The most common are plate absorbers, packed absorbers, falling film absorbers, spray absorbers, *etc.*

Although packed columns are the most common gas-liquid contact facilities used in the chemical industry, they suffer from various operating problems in some applications. For example, in NH_3 stripping, the formation of nitrate deposits on packing materials results from the biological oxidation of NH_3. Moreover, the dust-laden gases produce solid deposits to finally clog the packing interstitial spaces.[14] In these applications, the sprayed columns are preferred because they offer many advantages over traditional towers, such as low pressure drop in the gas phase, simpler mechanical construction with low equipment costs, and a wide range of liquid/gas charge rates.[15] Naturally, their mass transfer performance depends on the physical properties of fluids, sprayed absorbents characteristics, such as their spatial distribution and droplets size.

In addition, the ability to divide the liquid into fine droplets (jet) through the nozzle depends on its geometric characteristics, such as main nozzle orifice, internal pressure, swirl chamber, cone angle of nozzle, as well as on the physicochemical properties of the liquid, such as surface tension, viscosity *etc.* A more detailed study on the effect of geometry on atomisation characteristics was presented by *Dafsari et al.*

However, their main disadvantage compared to packed towers is their low mass transfer efficiency due to the possible droplets coalescence, and consequently a significant reduction in interfacial area.[16]

In addition to the contact mode between phases in circulation, the equilibrium data of the working couple undoubtedly affect the efficiency of mass transfer in the absorber. From a pure kinetic point of view, the mass transfer between phases is dependent on the affinity between constituents of the phases.[17] The transfer intensity is measured by the flow rate through the interfacial area of the column, so that its analytical expression is given by:

$$\dot{N} = k_L a \cdot \left(x_i - x_\infty\right) = k_G a \cdot P_{tot}\left(y_\infty - y_i\right) \quad (6)$$

The rate of mass transfer by unit of volume ($\dot{N}$) is a measure of the transfer flow rate. Its unit is kmol m^{-3} s^{-1} and P_{tot} operating total pressure. This analytical expression consists of:

x_i and y_i – the compositions of the diffusing particle, *i*, at the interface, which are given by the equilibrium curve;

x_∞ and y_∞ – the specie compositions of the liquid and gas phases (bulk phase), respectively.

Fig. 2 presents the equilibrium curve, the operating line and other parameters.

This is the double film model where k_L is the individual coefficient of mass transfer liquid side, k_G is the individual coefficient of mass transfer, gas side, and *a* is the interfacial area *per* unit volume of the contactor.[18] To size these contactors and based on experimental results, the dimensional analysis makes it possible to establish correlations between the mass transfer coefficients and the hydrodynamic conditions of fluid flow rates in the form of exponential laws. Their expressions are presented:[19]

$$Sh = \alpha \cdot Re^b \cdot Sc^c \quad (7)$$

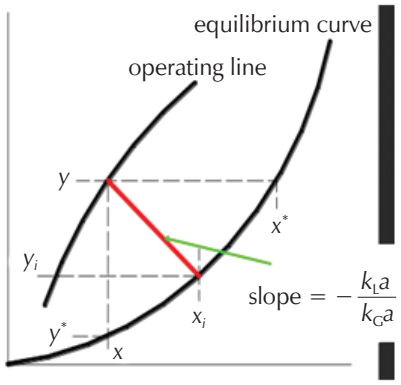

Fig. 2 – Schematisation of gas-liquid absorption in the contactor

Eq. (7) is a correlation used in mass transfer field to calculate the mass transfer coefficient in various contactors, where Sh is a dimensionless Sherwood number expressing the ratio of the mass rate transferred by convection to the mass flux transferred by molecular diffusion. Its expression is: $Sh = k_L D_c/\mathcal{D}$ where k_L is the mass transfer coefficient, D_c is the exchange characteristic length in the contactor, and $\mathcal{D}$ is the molecular diffusion coefficient.

Re is a dimensionless Reynolds number expressing the ratio of inertial forces to viscous forces. It has the expression: $Re = v_{ave} \cdot D_c/\mathcal{D}$ where v_{ave} is the average velocity of the flow, and *v* is the kinematic viscosity of the fluid.

Sc is a dimensionless Schmidt number. Its expression is: $Sc = \nu/\mathcal{D}$. It expresses the ratio of momentum viscous diffusion to mass diffusion flow rate.

α, b, and c are the constants that will be generally determined on the basis of experimental data for any contactor.

Another equivalent form:[20]

$$k_G a = \beta \cdot \dot{L}^r \cdot \dot{G}^n \quad (8)$$

where β, r, and n are the constants that will be equally determined on the basis of experimental data for any contactor.

Table 1 groups a few correlations relating to the usual systems used in absorption processes.

Analysis of the literature data shows that the absorption of water vapour by aqueous LiBr solutions is of the physical type.[25] For high LiBr concentrations, absorption can be limited by crystallisation problems with the release of large amounts of heat because that is an exothermal process. To improve the absorber performance in the A.C., this study was carried out with a view to prospecting the impact of various operating conditions on the mass transfer coefficients $K_G \cdot a$ and k_L, and therefore on the absorber size. Correlations are developed to estimate the overall coefficient of mass transfer as a function of gas and liquid flow rates, but also as a function of the average size of droplets at the outlet of the ejector holes.[26]

Table 1 – Correlations developed in absorption processes

Type of contactor	Binary system	Correlations between mass transfer coefficient and fluids flow rates	Application field	References
Plate with falling film	H_2O/LiBr	$K_G = \mathrm{Sh}\cdot\frac{\mathcal{D}}{\delta_F} = \left(\frac{1}{1-x_{H_2O}}\right)\cdot\frac{40}{11}\cdot\frac{\mathcal{D}}{\delta_F}$	Chilling by absorption	29
Spraying of liquid jet in a Venturi	Absorption of SO_2 by aqueous solution of NaOH	$K_G\cdot a = \left(\dot{G}/P_{tot}\right)\cdot\ln\left(y_e/y_s\right)$	Gas absorption	21
Falling film	H_2O/LiBr	$K_G = \frac{\dot{L}\cdot(y_s - y_e)/y_s}{(\rho_L\cdot a\cdot y)}$	Chilling by absorption	22
With vertical smooth tubes	H_2O/LiBr	$K_G = \frac{\dot{G}\cdot\left(\left(x_e^* - x_e\right) - \left(x_s^* - x_e\right)\right)}{\rho_L\cdot\ln\frac{\left(x_e^* - x_e\right)}{\left(x_s^* - x_s\right)}}$	Chilling by absorption	23
Sprayed column and falling film	air – NH_3/H_2O	$K_G\cdot a = 1.97\cdot\dot{G}^{0.71}\cdot\dot{L}^{0.54}$	Chilling by absorption	19
Falling film	H_2O/LiBr NH_3/H_2O	$K_G = \frac{\dot{G}}{\rho_L\cdot\ln\left(1-x_{avg}\right)/\left(1-x_i\left(T_{int},P\right)\right)}$	Chilling by absorption	24

1.2 Theoretical development of the operating absorber

In the absorber and through the gas-liquid interface, the gaseous solute (A) diffuses to be absorbed physically or chemically. The overall material transfer coefficients ($K_G\cdot a$ and $K_L\cdot a$) were used to quantify the transferred mass flow rate, and find relations between their variation with the flow rates as well as with the droplets size at the outlet of the ejector, d_G. Indeed, many previous works, relating to spray towers, have focused on the treatment of the mass transfer coefficient. *Codolo et al.*,[23,24] *Ma et al.*,[26] and *Zeng et al.*[27] have experimentally determined the mass transfer coefficient and established empirical correlations. Given its electrolytic aspect, it is mentioned that the mixture liquid deviates from the behaviour of an ideal solution where the thermodynamic activity to the place of the concentration was introduced.[28] With the concept of overall mass transfer coefficients, the mass balance can be expressed by the following equations:[19]

$$\dot{N} = K_L\cdot a\cdot\left(C^*_{H_2O} - C^{\infty}_{H_2O}\right) = K_G\cdot a\cdot\left(P^{\infty}_{H_2O} - P^*_{H_2O}\right) \qquad (9)$$

where K_L and K_G are the overall coefficients of mass transfer for sided gas and sided liquid, respectively. The $C^*_{H_2O}$ and $P^*_{H_2O}$ are the water concentration and partial pressure of water vapour at the equilibrium in both phases. Moreover, the $C^{\infty}_{H_2O}$ and $P^{\infty}_{H_2O}$ are the concentration and partial pressure of water vapour in both bulk phases, respectively.

Depending on the saturated vapour pressure of the solute, $P^0_{H_2O}$, the partial pressure in the gas phase is given by Raoult's law for a real solution:

$$P^{\infty}_{H_2O} = \gamma_{H_2O}\cdot x_{H_2O}\cdot P^0_{H_2O} \qquad (10)$$

where γ_{H_2O} is the activity coefficient of water in the liquid water-LiBr solution which is a non-ideal mixture. The x_{H_2O} and P^0_A are mole fraction of the water in the liquid phase and saturated vapour pressure of pure water at the mixture temperature, respectively.

In general, these activity coefficients depend on the temperature and the composition of the phases (Laws of Margules, Wilson, Van Laar, NRTL, *etc.*).[29] Moreover, depending on the value of the slope of the equilibrium curve, the Henry's law constant (He), we distinguished:

1) He≪1, the gas phase controls the mass transfer kinetics. In practice, this means that the design of the absorber must consider this by favouring the use of packed absorbers as well as the spray towers with the contribution to increasing the exchange specific area between phases.
2) He≫1, the resistance to mass transfer is located in the liquid phase. In practice, the design of the contactor should improve the mass transfer in the liquid phase under the action of mechanical agitation.

Since water vapour is very soluble in the electrolytic solution (water-LiBr), the liquid side mass transfer resistance is negligible. As a result, absorption is controlled by the gas phase.[15] It follows that the individual coefficient of mass transfer in the gas phase k_G, can be assimilated to the overall coefficient of mass transfer on the gas side, K_G:[19]

$$K_G \cong k_G \qquad (11)$$

1.3 Sizing of the tower

Modelling of the absorber functioning

Given the two modes of contact between phases throughout the absorber (droplets and wetted wall with water vapour), the operating model of the spray tower is based on some simplifying assumptions:

1) In the first section, of length, Z_G, the droplets are confined in the domain defined by the angle of the ejection nozzle cone. Their distribution is uniform on any cross-section of the contactor.
2) In the second section, the film trickles down the wall to constitute the wetted zone, and the thickness of the liquid film, δ_F, is constant along the length, Z_F.
3) Following the coalescence phenomenon, the majority of the droplets clump in the wetted wall. The contribution of this latter to the exchange interfacial area in the liquid film, a_F, is relatively small. Consequently, the mass transfer *via* the droplets is insignificant.
4) No preferential flowing for the gas stream.
5) The solute concentration in the circulating phases undergoes appreciable variations through the absorber.
6) The equilibrium curve is a straight line.

The liquid solution is sprayed strongly through the ejector under the pressure effect, P_{ejct}, in fine droplets, which are dispersed in the column within the ejection angle of the cone, 2θ, along height Z_G. In this section, the contact between the rising gas and the falling droplet conduces to the absorption of water vapour. This mass transfer is accompanied by a progressive increase in the size of the droplets. These follow their falling to the bottom of the column, while others collide with the wall to form a film the thickness of which is assumed constant after a short length (the entry effect in the liquid film).

In this last section, the mass exchange is sufficiently intensive between the gas stream (inert + water vapour) and the dripping film. At different levels of the column, and taking into account the exothermic nature of the absorption of water vapour by the aqueous LiBr solution (high heat of mixing), there is a significant rise in temperature which should compromise the intensification of the process. The gas velocity, depending on the diameter of the spray tower, must be low so as not to entrain the droplets in an upward movement and lead to tower flooding. From a practical standpoint, a velocity 20 % of the droplet's free falling velocity would be useful to estimate the tower diameter. However, the free falling velocity is dependent on the drag coefficient.[17]

1.4 Estimation of the lengths of exchange zones

The sizing of the apparatus must take into account the hydrodynamics of fluids flowing in the column and its mass transfer performance, based on the liquid vapour equilibrium data between phases. The droplet falling velocities as well as their initial diameters are entirely depending on the outlet conditions of the ejector (pressure and diameter).

Spraying area: From a geometric point of view and based on tower diameter, D_t, the height of the spraying area, Z_G, should be determined from the angle of the spray nozzle cone (Fig. 3) using the following relation:

$$Z_G = \frac{D_t}{(2 \cdot \tan \theta)} \tag{12}$$

In spraying zone, a_d is the exchange interfacial area from droplets. Given that $\dot{G}$ and $\dot{L}$ are the flow rates of inert in the two streams and that the mass transfer coefficient, $K_G \cdot a_d$ is an accessible amount experimentally, the molar concentrations of solute, y_{SF} and x_{SF}, in the column (Fig. 3), are obtained by simultaneously solving the following algebraic equations:

$$Z_G = \frac{\dot{G} \cdot (y_{SF} - y_s)}{K_G \cdot a_d \cdot P_{tot} (y - y^*)_{lm}} \tag{13}$$

Note that a_d can be estimated based on considerations reporting to the droplets average diameter, d_G.[19] Thus, we have:

$$a_d = \frac{4 \cdot \dot{n}_G \cdot d_G^2}{D_t^2 \cdot Z_G} \tag{14}$$

where $\dot{n}_G$, is the number of droplets flowing *per* unit of time. Depending on the liquid flow rate and the average diameter of the droplet, d_G, it is written:[1]

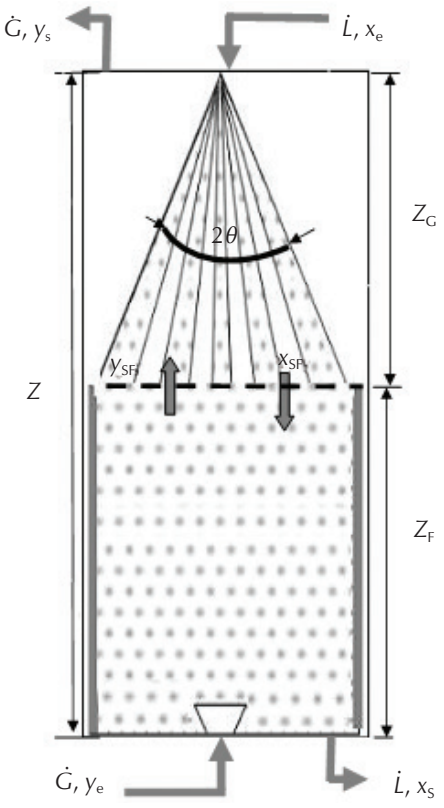

Fig. 3 – Modelling of mass transfer in the spray tower

$$\dot{n}_G = \frac{6\dot{L}}{\pi d_G^3} \tag{15}$$

The operating line equation can be written as:

$$y_{SF} = \frac{\dot{L}}{\dot{G}}\left(x_{SF} - x_e\right) + y_s \tag{16}$$

where x_e, y_s are the molar fraction inlet of liquid phase in the spraying zone and the molar fraction outlet of gaseous phase from spraying zone, respectively.

Film zone: In steady state, the mass balance over the gas phase along a differential element of height, dz, can be written as:

$$\dot{G}dy = \dot{N} \cdot a_F \cdot dz = K_G \cdot a_F \cdot P_{tot} \cdot \left(y - y^*\right) \cdot dz \tag{17}$$

We will assume that the absorption takes place in the liquid film. At constant pressure and temperature, and according to the Fig. 5, the height of this section, Z_F, is:[19]

$$Z_F = \left(\frac{\dot{G}}{K_G \cdot a_F \cdot P_{tot}}\right)\frac{y_e - y_{sF}}{(y - y^*)_{lm}} \tag{18}$$

where a_F is the specific area of mass exchange, film sided, which can be estimated based on the film thickness, δ_F, and on the geometrical parameters of the tower. The result is given by *Treybal*:[18]

$$\delta_F = \left[\frac{3\mu_L \cdot \dot{L}}{\pi \cdot D_t \cdot \rho_l^2 \cdot g}\right]^{\frac{1}{3}} \tag{19}$$

Thus, a_F is:

$$a_F = \frac{\left(D_t - 2 \cdot \delta_F\right)}{\delta_F \cdot \left(D_t - \delta_F\right)} \tag{20}$$

In Eq. (13), K_G can be correlated to some experimental data (gas and liquid flow rates in the tower with wetted walls).[19] Therefore, the total height of the spray tower can be calculated from:[1,18]

$$Z = Z_G + Z_F \tag{21}$$

2 Experimental part

2.1 Presentation of absorber prototype

The spray column is a gas-liquid counter current contactor designed for the treatment of polluted gaseous effluents for its mass transfer performances. Thus, we designed a polyvinyl chloride (PVC) column, of circular cross-section, for reasons relating to the low cost of the material and its chemical stability under the expected operating conditions.

The transparent appearance of the material made it possible to visualise the hydrodynamics of the flowing fluids (droplets and film) inside the column, and therefore to discern the contact modes between phases. The dimensions of the column were diameter D_t = 10 cm, height Z_t = 10 cm (Fig. 4).

Fig. 4 – Representative photo of the experimental installation

2.2 Acquisition of experimental data

Experimentation was carried out according to the following:

1) Fixing the operating pressure in the column to atmospheric pressure.
2) Preparation of the aqueous solution by dissolving in distilled water the LiBr, anhydrous crystalline solid, produced by the Alfa Aesar Laboratory, with a purity of 99 %, molar mass M = 86.85 g mol^{-1}, and a density d = 3.464.
3) Fig. 5 shows the overall layout of the experimental set-up.
4) The flow rate of the LiBr solution, $\dot{L}$, was measured by a flow meter of the HEIDOLH PUMPDRIVE 5001 type. This aqueous solution was sprayed through a liquid distributor, in the form of a circular plate, provided with 17 slots, distributed uniformly (Fig. 6).
5) At the different sections of the column, the droplets size (diameter) was directly read on a photograph taken on the descending jet.
6) The temperature of the LiBr feed solution was measured continuously by means of digital thermometer, type IP 65 WATER PROOF PT 100.

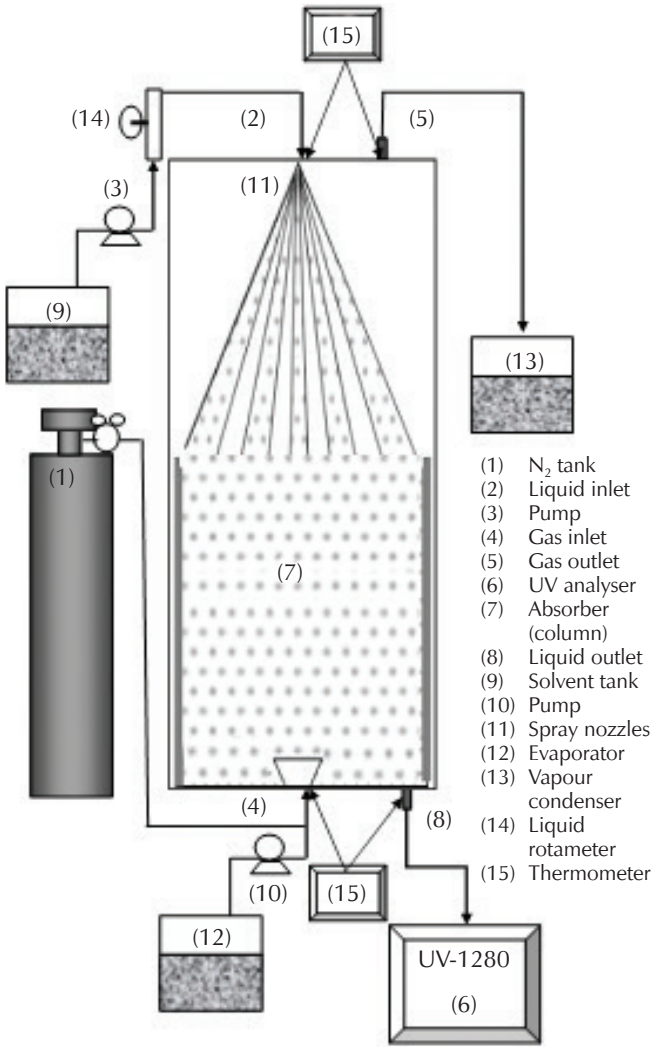

Fig. 5 – Schematic diagram showing the overall layout of the experimental setup

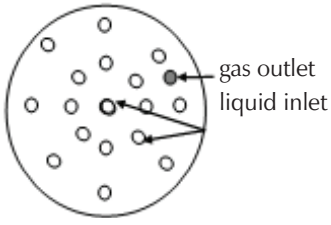

Fig. 6 – Schematic diagram showing top layout

The water vapour was entrained by a stream of nitrogen gas, with a flow rate, $\dot{G}$, and injected at the bottom of the column through an appropriate gas distributor. At contact of both fluids circulating counter currents in the column, the water vapour was physically absorbed by the aqueous LiBr solution.

To carry out the experiments and record the different operating conditions, the column was fitted with the following operating accessories:

1) Hydraulic pump, type HEIDOLH PUMPDRIVE 5001, for the circulation of the absorbent solution of LiBr;
2) Digital thermometers, IP 65 WATER PROOF PT 100, to measure the inlet and outlet temperatures of the two fluids circulating in the column;
3) A device SHIMADZU UV-1280 to measure the LiBr content of the outlet liquid solution, x_s.

Results and discussion

The mass transfer in the column is influenced by the physical state of the fluids and their transport properties (flow rates, phase inlet concentrations, diffusivity coefficient, viscosities, *etc.*). Operating at atmospheric pressure (P_{tot} = 1 atm), the experiments were carried out by varying the following operating amounts: flow rate of solution, L; flow rate of gas $\dot{G}$; liquid phase concentration, x_e; vapour phase concentration, y_e, and inlet streams temperatures.

Theoretically, for the analysis of the feasibility of the absorption process, the equilibrium data of the water-LiBr binary system is to be developed while using the osmotic coefficient method. Moreover, Dalton's law applied to the gaseous phase, assumed ideal, makes it possible to express the partial pressure of water vapour, $P^{\infty}_{H_2O}$, by the following relation;

$$P^{\infty}_{H_2O} = y_{H_2O} \cdot P_{tot} \tag{22}$$

where y_{H_2O} is the molar fraction of the water in the gaseous phase.

After simple combination with Eq. (10), the equilibrium equation can be written:

$$y_{H_2O} = \frac{\gamma_{H_2O} \cdot P^0_{H_2O}}{P_{tot}} \cdot x_{H_2O} \tag{23}$$

The functional analysis of the expression of y_{H_2O} allows us to note that it is dependent on both temperature and composition at equilibrium. Given the operating conditions of the A.C., the pressure at the absorber can be fully determined by reading directly on the Oldham's diagram (Appendix B) of the binary system (water-LiBr). From the Eq. (23), the $y_{H_2O} = f(x_{H_2O})$ expresses the equilibrium relation the slope of which is the Henry constant, He. We can define it by the following expression:

$$\mathrm{He}\left(T, x_{H_2O}\right) = \frac{\gamma_{H_2O} \cdot P^0_{H_2O}}{P_{tot}} \tag{24}$$

In previous parts, it was mentioned that the absorption process of water by aqueous solution of lithium bromide is strongly exothermic. Consequently, work with concentrated solutions must be avoided in order to maximize the mass transfer in the contactor. For example, a temperature close to 140 °C leads to He = 1.01 and it cannot be decided where the mass transfer resistance is situated. This affirmation confirms the good choice of the operating

temperature, where the gas phase mainly controls the mass transfer kinetics. In practice, this means that the absorber design must consider this by favouring the use of packed absorbers as well as sprayed towers of the liquid phase in order to contribute to the increase in the exchange specific area between phases. Thus, at operating pressure, the analysis of the effect of the various operating variables of the absorber can be approached carrying out the following experimental study.

3.1 Flow rate of LiBr solution and its impact on droplet size

For pump power of the solution equal to 150 W, the diameter of the droplets was read directly on the photograph taken on the downward liquid jet at the different sections of the column (Fig. 7). The results showing the variation of the droplets diameter with the flow rate are presented in Fig. 8.

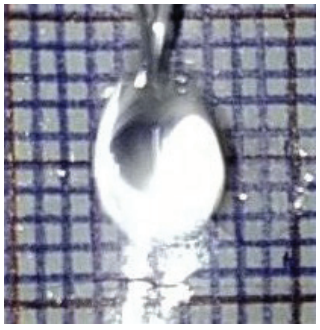

Fig. 7 – Experimental determination of the dimension of the droplets

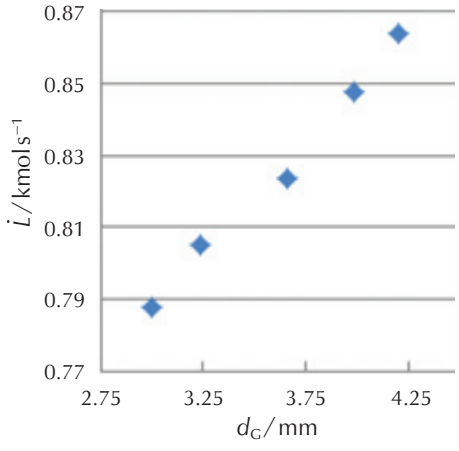

Fig. 8 – Variation of the droplets diameter *vs* the solution flow rate

To model the operation of the column taking into account the droplet size, we correlated the data $\dot{L} = \dot{L}(d_G)$ by proposing an exponential law. For a vapour flow rate $\dot{G} = 0.012$ kmol s^{-1}, the parametric identification made it possible to establish the following regression:

$$\dot{L} = 1.340 \cdot (d_G)^{0.407} \tag{25}$$

It may be seen that the size of the descending drop increased with the axial position along the column (Fig. 9). Such a growth trend is quite predictable given the affinity and hygroscopicity of the lithium bromide solution to the water vapour.[30] Indeed, by absorption, the water vapour condensed to contribute to the increase in droplets size. However, the axial rate of this growth was more pronounced at the bottom of the column than at its upper part, *i.e.,* the lower part of the column is more active in terms of absorption.

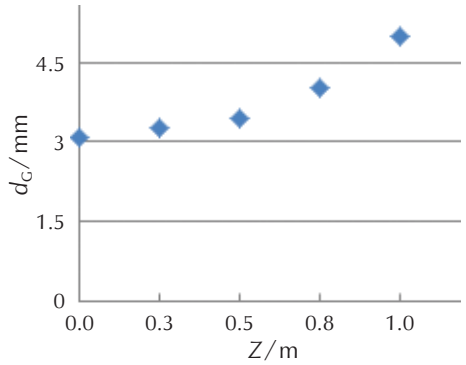

Fig. 9 – Axial profile of the droplets diameter through the tower

3.2 Aqueous solution flow rate effect

For an absorber operating in a black box, and taking into account the low concentrations solute in the two streams, we expressed the compositions in molar fractions. Throughout the contactor, the mass balance can establish the operating line, according to equation:

$$y_s = \frac{\dot{L}}{\dot{G}}(x_e - x_s) + y_e \tag{26}$$

It should be mentioned that the absorption of water vapour by the solution is a strongly exothermic operation with a heat of mixing expressed by the relation.[31]

$$\overline{h}^{Ex}_{(T,P,x_{LiBr})} = \\ = -x_{LiBr} \cdot \nu \cdot R \cdot T^2 \left(\frac{M_{H_2O}}{M_{LiBr}}\right) \cdot \left(\sum_{i=1}^{6} \frac{2}{i} \cdot \left(\frac{\partial a_i}{\partial T}\right) \cdot I^{i/2} + \sum_{i=2}^{3} \left(\frac{P_{tot}}{\nu} \cdot \frac{\partial b_i}{\partial T}\right) \cdot I^{i/2}\right) \tag{27}$$

where ν is the dissociation number (=2 for LiBr), I is the concentration expressed in molality, and a_i, b_i are the coefficients of polynomial law of Kim and Ferreira.[32]

As an indication and for an intermediate concentration of $x_{LiBr} = 0.50$, and at a temperature $T = 132$ °C, the mixing heat was $\overline{h}^{Ex}_{(T,P,x_{LiBr})} = 3029.1$ kJ kmol^{-1}. This positive thermodynamic amount resulted in an increase in solution

temperature, and the thermodynamic equilibrium was displaced to negatively affect the absorption capacity of the column while eventually causing crystallization (Oldham's diagram).

For the operating conditions of the absorber, we studied the influence of the flow rate of the LiBr aqueous solution on its performance. The results are presented in Fig. 10. By analysing the influence of $\dot{L}$, we noticed that the composition of the gas phase, at outlet of the column, had seriously decreased for high flow rates $\dot{L}$. Furthermore, depending on the exchanged quantity, the overall material transfer coefficient, $K_G \cdot a$, is expressed by the integral equation of the transfer kinetics:

$$K_G \cdot a = \frac{\dot{G} \cdot (y_e - y_s)}{P_{tot} \cdot S \cdot Z (y - y^*)_{ml}} \tag{28}$$

where $(y - y^*)_{lm}$ is the logarithmic mean of composition, defined by:

$$(y - y^*)_{lm} = \frac{(y_e - y_e^*) - (y_s - y_s^*)}{\ln\left(\frac{y_e - y_e^*}{y_s - y_s^*}\right)} \tag{29}$$

To study the influence of the solution liquid flow rate on the absorber performance, we followed the variation in the water content of the streams at both extremities of the column while measuring water concentration for:

1) The liquid phase by UV spectrophotometric analysis;
2) The gas phase, y_e, was determined by material balance on the amount of evaporated water, while y_s was given by the amount of condensed water, at the outlet of the absorber.

The experimental data allowing the analysis of the flow rate liquid impact on the phases composition, and the overall coefficient of mass transfer sided gas are presented in the Table 2.

The analysis results, expressing the variation of the water content through the column, for different flow rate ratios ($\dot{L}/\dot{G}$) are given in Fig. 10. As an implicit function of the liquid flow rate, $\dot{L}$, and by exploiting the relation (18), the variation of the $K_G \cdot a$ is given by Fig. 11.

After opting for the exponential law for the functional relation, $K_G \cdot a = f(\dot{L})$, and a vapour flow rate $\dot{G} = 0.012$ kmol s^{-1}, the parametric identification method applied to the experimental results gives:

$$K_G \cdot a = 7.61 \cdot \dot{L}^{0.543} \tag{30}$$

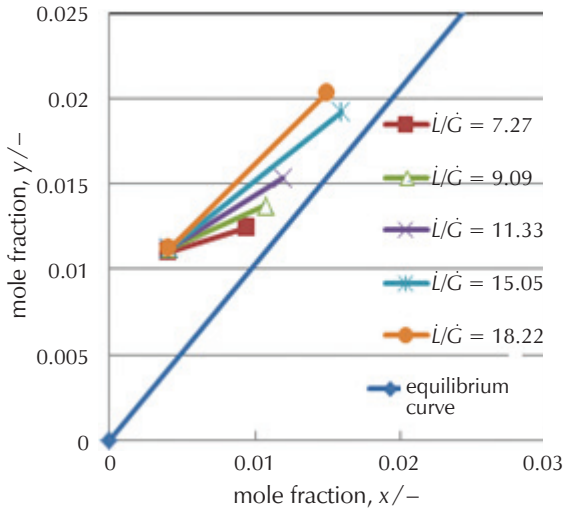

Fig. 10 – Influence of ($\dot{L}/\dot{G}$) on the capacity of the absorber

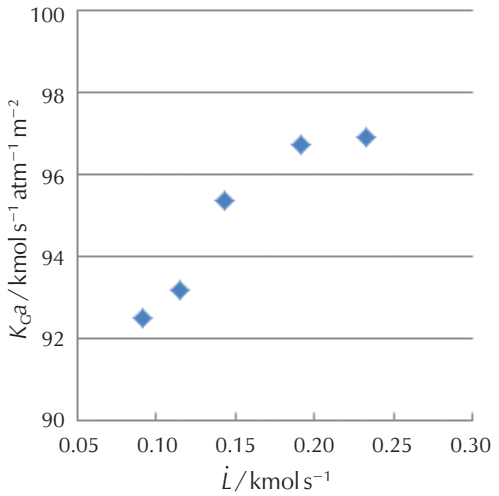

Fig. 11 – Effect of flow rate of LiBr solution on mass transfer conductance. $P_{tot} = 1$ atm, $\dot{G} = 0.012$ kmol s^{-1}

Moreover, $K_G \cdot a$ can be related to the droplet diameter at the outlet of the ejector. This relation can be written:

$$K_G \cdot a = 8.921 \cdot (d_G)^{0.221} \tag{31}$$

Similarly, for systems where the resistance in the gas phase predominates, such as in the air – NH_3/H_2O system,[33] it was found that the mass transfer coefficient increased with the increase in gas and liquid flow rates.

Table 2 – Listing of flow rates of phases in the absorber

$\dot{G} = 0.012$ kmol s^{-1}, $x_e = 0.0037$, $y_e = 0.0115$					
$\dot{L}$ / kmol s^{-1}	0.09191321	0.11489151	0.14361439	0.19148585	0.23199248

3.3 Effect of water vapour flow rate

The experimental data allowing the analysis of the flow rate vapour impact on the phases' composition, and the overall coefficient of mass transfer sided gas are presented in Table 3.

Table 3 – Listing of gas flow rate and its composition for absorber analysis

$\dot{L}$ = 0.073 kmol s^{-1}, x_e = 0.005					
$\dot{G}$ = 0.012 kmol s^{-1}	0.0127	0.0130	0.0131	0.0132	0.0133
y_e	0.092	0.145	0.184	0.205	0.219

Fig. 13 shows the evolution of the composition of the phases (liquid and vapour) circulating through the absorber for a liquid flow rate $\dot{L}$ = 0.073 kmol s^{-1}. It appears that, for a given liquid phase composition, the water vapour composition remains invariable regardless of the vapour flow rates because the operating lines are practically superimposed.

Through these first experimental results, we calculated the mass transfer conductance using the mass balance Eqs. (26) and (28).

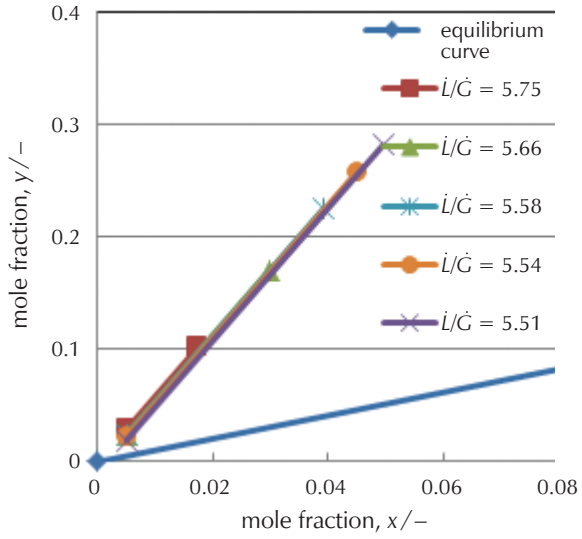

Fig. 12 – Influence of the composition of the phases (liquid and vapour) circulating through the absorber $\dot{L}$ = 0.073 kmol s^{-1}

These results show that the mass transfer coefficient, $K_G \cdot a$, increased with increasing water vapour flow rate, and that the transfer intensity is favoured by the exchange interfacial area in the contactor. In order to numerically analyse and correlate these data, we applied a linear regression law. The parametric identification made it possible to establish the relationship:

$$K_G \cdot a = 0.2631 \cdot \dot{G}^{0.363} \qquad (32)$$

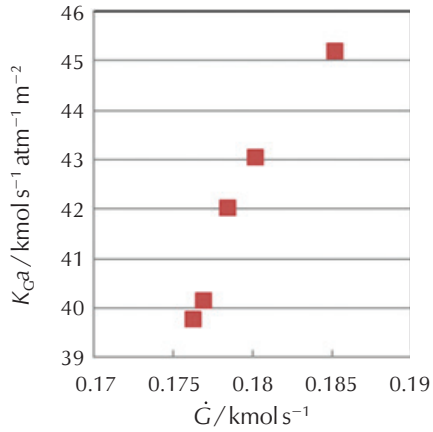

Fig. 13 – Effect of water vapour flow rate on overall mass transfer coefficient, P_{tot} = 1 atm, $\dot{L}$ = 0.073 kmol s^{-1}

Graphically, and for different hydrodynamic operating conditions, the transfer coefficient in kmol s^{-1} atm^{-1} m^{-2} kept values within a restricted interval [0.0398, 0.0452].

4 Conclusion

The performances of absorption machines in refrigeration mode remain, principally, dependent on the intensity of the mass transfer in the absorber. In this work, an absorber, sprayed tower type, was studied taking into account the thermodynamic aspects and the liquid-vapour equilibrium within an absorption machine using the H_2O/LiBr couple. The spray absorber sizing methodology was proposed in order to calculate the height of the two sections based on the liquid-vapour equilibrium data. For an average operating temperature of the absorber and at atmospheric pressure, the equation of the equilibrium curve was a straight line, of which Henry's is practically constant with a vapour phase moderately controlling the mass transfer.

For a vapour flow rate, $\dot{G}$ = 0.012 kmol s^{-1}, and for an ejection pump constant power of 150 W, the experimental results showed that the diameter of the droplets leaving the ejection nozzle increased with the flow rate of the liquid according to an exponential regression law. Moreover, the size of the descending droplets underwent a fairly pronounced growth with the axial position along the column taking into account the hygroscopicity of the solution. The results relating to the variation of the $K_G \cdot a$ values *versus* the liquid flow rate, $\dot{L}$, were given by the relation $K_G \cdot a = 7.61 \cdot \dot{L}^{0.543}$. In addition, $K_G \cdot a$ was less affected by the flow rate of gaseous stream according to a law of the type: $K_G \cdot a = 0.2631 \cdot \dot{G}^{0.363}$.

Based on the experimental results, and in order to contribute to mass transfer intensification, it is interesting to choose the absorber operating conditions by opting for high liquid flow rates, and incorporate a heat exchanger in the film dripping using the adequate refrigerant to lower the temperature which compromises the mass transfer.

ACKNOWLEDGEMENTS

The authors acknowledge the financial support of the General Directorate of Scientific Research and Technological Development (G.D.S.R.T.D.) at the Ministry of Higher Education and Scientific Research, Algeria, for their assistance in the realization of this work.

List of abbreviations and symbols

COP – coefficient of performance, –

D_t – spray tower diameter, m

$\dot{G}$ – gas flow rate, kmol s^{-1} or kg s^{-1}

He – slope of the equilibrium curve, –

K_G – overall gas phase mass transfer coefficient, kmol atm^{-1} m^{-2} s^{-1}

K_L – overall liquid phase mass transfer coefficient, m s^{-1}

$\dot{L}$ – liquid flow rate, kmol s^{-1} or kg s^{-1}

$H_L^{T_E}$ – latent heat of water vaporization, kJ kg^{-1}

M – molecular mass, kg kmol^{-1}

$\dot{N}$ – flow rate of exchanged mass, kmol s^{-1} m^{-3}

P_{tot} – operating pressure of the tower, atm

P_{ejct} – ejector pressure, atm

$\dot{Q}_A$ – thermal power exchanged at absorber, kW

$\dot{Q}_C$ – thermal power exchanged at condenser, kW

$\dot{Q}_G$ – thermal power exchanged at generator, kW

$\dot{Q}_E$ – thermal power exchanged at evaporator, kW

R – universal gas constant, kJ kmol^{-1} K^{-1}

Re – Reynolds number, –

Sc – Schmidt number, –

Sh – Sherwood number, –

T – temperature, K

T_{int} – temperature at the interphase, K

$\dot{W}_p$ – power of the pump, W

Z – total height of spray tower, m

Z_F – height of wetted-wall, m

Z_G – height of spray zone, m

a – interfacial area of mass transfer, m^2 m^{-3}

d_G – droplet diameter

a_G – specific area of droplets, m^2 m^{-3}

$k_G \cdot a$ – gas film side mass transfer coefficient, kmol atm^{-1} m^{-2} s^{-1}

$k_L \cdot a$ – liquid film side mass transfer coefficient, kmol m^{-2} s^{-1}

l – molality, mol kg^{-1} of solvent

$\dot{n}_G$ – number of droplets per time unit, s^{-1}

a_F – exchange interfacial area of film zone, m^2 m^{-3}

D – diffusivity of water in solution aqueous LiBr, m^2 s^{-1}

$C^*_{H_2O}$ – water concentration at equilibrium, kmol m^{-3}

$C^\infty_{H_2O}$ – water concentration in bulk phase, kmol m^{-3}

$P^\infty_{H_2O}$ – partial pressure of water vapour in bulk phase, atm

$P^*_{H_2O}$ – partial pressure of water vapour at equilibrium, atm

P^0_{eau} – saturated vapour pressure of pure water, atm

x_{avg} – average concentration of liquid in falling film, –

γ_{H_2O} – activity coefficient of water, –

$\overline{h}^{Ex}_{(T,P,x_{LiBr})}$ – heat of mixing, kJ kmol^{-1}

a – interfacial exchange area *per* unit volume, m^2 m^{-3}

α – constant, –

b – constant, –

c – constant, –

β – constant, –

r – constant, –

n – constant, –

y_{SF} – molar fraction inlet of gaseous phase to spraying zone, –

x_{SF} – molar fraction outlet of liquid phase from spraying zone, –

y_{H_2O} – molar fraction of the water in gaseous phase, –

x_{H_2O} – molar fraction of the water in liquid phase, –

y_s – molar fraction of the water at outlet from gaseous phase, –

y_e – molar fraction of the water at inlet in gaseous phase, –

x_s – molar fraction of the water at outlet from liquid phase, –

x_e – molar fraction of the water at inlet in liquid phase, –

Φ – osmotic coefficient, –

ν – dissociation number, –

$*$ – saturated state of pure solvent, –

θ – spray cone angle, °

ρ_l – density of liquid, kg m^{-3}

δ_F – thickness of liquid film, m

μ_L – dynamic viscosity of liquid phase, kg m^{-1} s^{-1}

e – inlet, –

s – outlet, –

APPENDICES

Appendix A

Calculation of the vapour pressure of pure water (Antoine's Law)

The saturated vapour pressure of pure water, P^0_{eau}, is related to temperature by the Antoine equation:[35]

$$\log p^{o}_{eau}\left(\text{mmHg}\right) = 8.1093 - \frac{1684.3}{T\left(^{\circ}\text{C}\right)+230} \qquad \text{(A.1)}$$

Vapour-liquid equilibrium of the water-LiBr system

Given the non-ideality of the aqueous LiBr solution, the activity coefficient of water was introduced *via* the equation of *R. Palacios et al.*:[33]

$$\log\left(\gamma_{H_2O}\right) = -\varnothing.v.I.M_{H_2O} \qquad \text{(A.2)}$$

where I, is the molality of the solution, calculated as a function of the mass fraction x_{LiBr} by the relation:

$$I = \frac{x_{LiBr}}{\left(1-x_{LiBr}\right)\cdot M_{LiBr}} \qquad \text{(A.3)}$$

If v is the dissociation number of the LiBr molecule, $\varnothing$ is the osmotic coefficient, given by Kim and Ferreira according to the polynomial law:[32]

$$\varnothing = 1+\sum_{i=1}^{6} a_i \cdot I^{i/2} + \frac{p_{tot}}{2\cdot v}\sum_{i=1}^{3} i\cdot b_i \cdot I^{i/2} \qquad \text{(A.4)}$$

a_i and b_i are given by the following equations:

$$a_i = \sum_{j=0}^{2} a_{ij}\cdot T^{-j} \qquad \text{(A.5)}$$

$$b_i = \sum_{j=0}^{2} b_{ij}\cdot T^{-j} \qquad \text{(A.6)}$$

The constants a_{ij}, b_{ij} are given in Table A1.

Table A1 – Values of a_{ij} and b_{ij} in the equation of *Kim et al.*[32]

Constants	$J=0$	$J=1$	$J=2$
a_{1j}	$-2.20\cdot 10$	$4.94\cdot 10^{3}$	$-6.55\cdot 10^{5}$
a_{2j}	$-3.81\cdot 10^{3}$	$2.61\cdot 10^{6}$	$-3.67\cdot 10^{8}$
a_{3j}	$1.23\cdot 10^{5}$	$-7.72\cdot 10^{7}$	$1.04\cdot 10^{10}$
a_{4j}	$-1.47\cdot 10^{6}$	$9.20\cdot 10^{8}$	$-1.19\cdot 10^{11}$
a_{5j}	$7.77\cdot 10^{6}$	$-4.94\cdot 10^{9}$	$6.32\cdot 10^{11}$
a_{6j}	$-1.51\cdot 10^{7}$	$9.84\cdot 10^{9}$	$-1.27\cdot 10^{12}$
b_{0j}	$-4.42\cdot 10^{-5}$	$3.11\cdot 10^{-2}$	-4.36
b_{1j}	$3.07\cdot 10^{-4}$	$-1.86\cdot 10^{-1}$	$2.74\cdot 10$
b_{2j}	$-4.08\cdot 10^{-4}$	$2.16\cdot 10^{-1}$	$-2.52\cdot 10$

In addition, the activity coefficient of LiBr is determined by numerical integration of the Gibbs-Duhem relation:

$$x_{H_2O}\cdot d\left(\ln\gamma_{H_2O}\right) + x_{LiBr}\cdot d\left(\ln\gamma_{LiBr}\right) = 0 \qquad \text{(A.7)}$$

The gas phase is assumed to be ideal and obey Dalton's law, while the liquid phase is governed by Raoult's law for a real solution. Thus, in gas phase, the water partial pressure has the expression:

$$P_{H_2O} = y_{H_2O}\cdot P_{tot} = \gamma_{H_2O}\cdot x_{H_2O}\cdot P^{0}_{H_2O} \qquad \text{(A.8)}$$

where x_{H_2O} and y_{H_2O} are the mole fractions of the component in the liquid and gas phases. Therefore, the constant of Henry He's law has the expression:

$$He = \frac{y_{H_2O}}{x_{H_2O}} = \frac{\gamma_{H_2O}\cdot P^{0}_{H_2O}}{P_{tot}} \qquad \text{(A.9)}$$

Appendix B

Oldham's Diagram of water-LiBr system.[35]

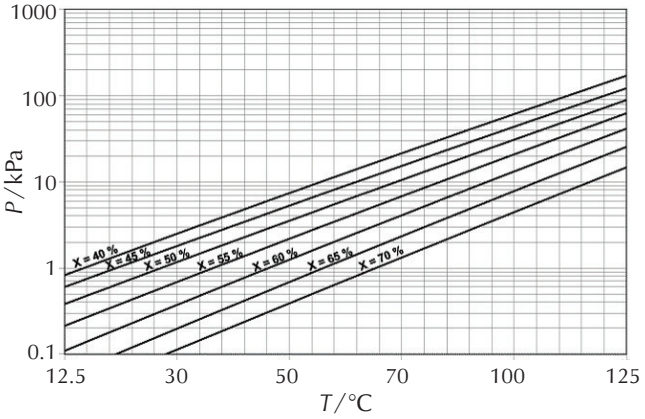

References
Literatura

1. *R. Tatin, L. Moura, N. Dietrich, S. Baig, G. Hébrard*, Physical absorption of volatile organic compounds by spraying emulsion in a spray tower: Experiments and modelling, Chem. Eng. Res. Des. **104** (2015) 409–415, doi: https://doi.org/10.1016/j.cherd.2015.08.030.
2. *S. Zhou, G. He, Y. Li, X. Liang, Q. Pang, D. Cai*, Comprehensive experimental evaluation of an exhaust-heat-driven absorption refrigeration cycle system using NH_3-NaSCN as working pair,Int. J. Refrig. **126** (2021) 168–180, doi: https://doi.org/10.1016/j.ijrefrig.2021.01.013.
3. *M. Arens, M. Åhman, V. Vogl*, Which countries are prepared to green their coal-based steel industry with electricity? – Reviewing climate and energy policy as well as the implementation of renewable electricity, Renew. Sust. Energ. Rev. **143** (2021) 110938, doi: https://doi.org/10.1016/j.rser.2021.110938.
4. *J. Famiglietti, T. Toppi, L. Pistocchini, R. Scoccia, M. Motta*, A comparative environmental life cycle assessment between a

condensing boiler and a gas driven absorption heat pump, Sci. Total Environ. **762** (2021) 144392, doi: https://doi.org/10.1016/j.scitotenv.2020.144392.

5. *Q. Ji, Z. Han, X. Zhang, X. Sun, G. Li, X. Li, L. Yang*, Study on the heating performance of absorption-compression hybrid heat pump in severe cold regions, Appl. Therm. Eng. **185** (2021) 116419, doi: https://doi.org/10.1016/j.applthermaleng.2020.116419.
6. *J. T. Gao, Z. Y. Xu, R.Z. Wang*, An air-source hybrid absorption-compression heat pump with large temperature lift, Appl. Energy **291** (2021) 116810, doi: https://doi.org/10.1016/j.apenergy.2021.116810.
7. *R. Tatin, L. Moura, N. Dietrich, S. Baig, G. Hébrard*, Physical absorption of volatile organic compounds by spraying emulsion in a spray tower: Experiments and modelling, Chem. Eng. Res. Des. **104** (2015) 409–415, doi: https://doi.org/10.1016/j.cherd.2015.08.030.
8. *A. Salazar, M. Prevost, R. Bugarel*, Economie d'énergie: pompe à chaleur à absorption, Int. J. Refrig. **4** (3) (1981) 126–130, doi: https://doi.org/10.1016/0140-7007(81)90103-1.
9. *R. Rivero, P. Le Goff*, Pompes à chaleur à distillation diabatique, Int. J. Refrig. **23** (1) (2000) 26–30, doi: https://doi.org/10.1016/S0140-7007(99)00030-4.
10. *Y. R. Fischer, J. C. C. Dutra, J. Rohatgi*, Thermodynamic modelling of a LiBr-H_2O absorption chiller by improvement of characteristic equation method, Int. J. Refrig. **120** (2020) 420–429, doi: https://doi.org/10.1016/j.ijrefrig.2020.06.030.
11. *R. Novella, V. Dolz, J. Martín, L. Royo-Pascual*, Thermodynamic analysis of an absorption refrigeration system used to cool down the intake air in an Internal Combustion Engine, Appl. Therm. Eng. **111** (2017) 257–270, doi: https://doi.org/10.1016/j.applthermaleng.2016.09.084.
12. *O. Kızılkan, A. Sencan, S. A. Kalogirou*, Thermoeconomic optimization of a LiBr absorption refrigeration system, Chem. Eng. Process. **46** (12) (2007) 1376–1384, doi: https://doi.org/10.1016/j.cep.2006.11.007.
13. *A. Laurent, J.-C. Charpentier*, Aires interfaciales et coefficients de transfert de matière dans les divers types d'absorbeurs et de réacteurs gaz—liquide, Chem. Eng. J. **8** (2) (1974) 85–101, doi: https://doi.org/10.1016/0300-9467(74)85012-4.
14. *W. S. Norman*, Absorption, Distillation and Cooling Towers, Longmans, London, UK, 1961.
20. *K. H. Javed, T. Mahmud, E. Purba*, Enhancement of mass transfer in a spray tower using swirling gas flow, Chem. Eng. Res. Des. **84** (6) (2006) 465–477, doi: https://doi.org/10.1205/cherd.05119.
16. *A. H. Lefebvre*, Atomization and Sprays, Hemisphere Publishing Corp., London, UK, 1984.
17. *P. A. Schweitzer*, Handbook of Separation Techniques for Chemical Engineers, 3rd edition, McGraw-Hill, New York, USA, 1997.
18. *R. E. Treybal*, Mass-Transfer Operations, 2nd edition, McGraw Hill, New York, USA, 1968.
19. *E. R. Gilliland, T. K. Sherwood*, Diffusion of vapors into air streams, Ind. Eng. Chem. **26** (5) (1935) 516–523, doi: https://doi.org/10.1021/ie50293a010.
20. *J.-F. Cap, S. Laga, C. Flores, B. Stutz*, Modélisation d'un absorbeur eau/bromure de lithium à film ruisselant en régime laminaire, Congrès annuel de la Société Française de Thermique (SFT), 28–31 May 2013, url: https://www.sft.asso.fr/Local/sft/dir/user-3775/documents/actes/congres_2013/articles/6194.pdf.
21. *A. Laurent, C. Fonteix, G. Besson, J.-C. Charpentier*, Aires interfaciales et coefficients de transfert de matière dans un laveur type à jet pulvérisé de liquide dans un Venturi, La Houille Blanche **65** (6-7) (1979) 443–449, doi: https://doi.org/10.1051/lhb/1979043.
22. *S. M. Deng, W. B. Ma*, Experimental studies on the characteristics of an absorber using LiBr/H_2O solution as working fluid, Int. J. Refrig. **22** (4) (1999) 293–301, doi: https://doi.org/10.1016/S0140-7007(98)00067-X.
23. *H. Takamatsu, H. Yamashiro, N. Takata, H. Honda*, Vapor absorption by LiBr aqueous solution in vertical smooth tubes, Int. J. Refrig. **26** (6) (2003) 659–666, doi: https://doi.org/10.1016/S0140-7007(03)00038-0.
24. *B. Narváez-Romo, M. Chhay, Elí W. Zavaleta-Aguilar, J. R. Simões-Moreira, A* Critical Review of Heat and Mass Transfer Correlations for LiBr-H_2O and NH_3-H_2O Absorption Refrigeration Machines Using Falling Liquid Film Technology, Appl. Therm. Eng. **123** (2017) 1079–1095, https://doi.org/10.1016/j.applthermaleng.2017.05.092.
25. *M. C. Codolo, W. A. Bizzo*, Experimental study of the SO_2 removal efficiency and volumetric mass transfer coefficients in a pilot-scale multi-nozzle spray tower, Int. J. Heat Mass Transf. **66** (2013) 80–89, doi: https://doi.org/10.1016/j.ijheatmasstransfer.2013.07.011.
26. *M. C. Codolo, W. A. Bizzo, R. Bertazzoli*, Performance of a UV-assisted hydrogen-peroxide-fed spray tower for sulfur dioxide abatement, Chem. Eng. Technol. **36** (7) (2013) 1255–1260, doi: https://doi.org/10.1002/ceat.201200699.
27. *S. C. Ma, B. Zang, H. H. Song, G. D. Chen, J. Yang*, Research on mass transfer of CO_2 absorption using ammonia solution in spray tower, Int. J. Heat Mass Transf. **67** (2013) 696–703, doi: https://doi.org/10.1016/j.ijheatmasstransfer.2013.08.090.
28. *Q. Zeng, Y. C. Guo, Z. Q. Niu, W. Y. Lin*, Volumetric overall mass transfer coefficients of CO_2 absorption into aqueous ammonia of fine spray, Proc. Chin. Soc. Electr. Eng. **31** (2) (2011) 45–50, doi: https://doi.org/10.1021/ie101821b.
29. *D. Zhao, C. Li, J. Liu, G. Zhou, Q. Zhang, C. Liu*, Experimental Assessment of Water Sprays Utilization for Controlling Hydrogen Sulfide Releases in Confined Space, Adv. Mater. Nanotechnol. Sustain. Energy Develop. Special issue **2015** (2015) 958252, doi: https://doi.org/10.1155/2015/958252.
30. *H. Noubli*, Développement d'un nouveau thermo-transformateur à absorption-démixtion: optimisation conjointe du cycle et du mélange de travail, Mémoire de doctorats, Institut National Polytechnique de Lorraine, Laboratoire Reactions et Genie des Procedes, 2010, url: https://hal.univ-lorraine.fr/tel-01748808.
31. *L. Labra, D. Juárez-Romero, J. Siqueiros, A. Coronas, D. Salavera*, Measurement of properties of a lithium bromide aqueous solution for the determination of the concentration for a prototype absorption machine, Appl. Therm. Eng. **114** (2017) 1186–1192, doi: https://doi.org/10.1016/j.applthermaleng.2016.10.162.
32. *D. S. Kim, C. A. Infante Ferreira*, A Gibbs energy equation for LiBr aqueous solutions, Int. J. Refrig. **29** (2006) 36–46, doi: https://doi.org/10.1016/j.ijrefrig.2005.05.006.
33. *R. Palacios-Bereche, R. Gonzales, S. A. Nebra*, Exergy calculation of lithium bromide–water solution and its application in the exergetic evaluation of absorption refrigeration systems LiBr-H_2O, Int. J. Energy Res. **36** (2) (2010) 166–181, doi: https://doi.org/10.1002/er.1790.
34. *A. Bandyopadhyay, M. N. Biswas*, Scrubbing of sulfur dioxide in a dual-flow scrubber, J. Indian Assoc. Environ. Manag. **25** (1998) 113–133.
35. *Y. Kaita*, Thermodynamic properties of lithium bromide–water solutions at high temperatures, Int. J. Refrig. **24** (5) (2001) 374–390, doi: https://doi.org/10.1016/S0140-7007(00)00039-6.

SAŽETAK

Utjecaj tehnologije raspršivanja na performanse apsorbera u H_2O/LiBr apsorpcijskom rashladnom uređaju

Wahiba Maouche,[a*] *Mustapha Douani*,[a] *Abdallah Labbaci*,[b] *Ümran Tezcan Ün*[c] i *Masoud Derakhshandeh*[d]

Posljednjih desetljeća vidljiv je stalan porast upotrebe rashladnih uređaja kod glavnih toplinskih motora koji se upotrebljavaju u industrijskim sektorima. Koeficijenti učinka apsorpcijskih rashladnih uređaja relativno su niski, a njihova isplativost ovisi o troškovima glavne opreme, točnije o cijeni apsorbera. U tijeku je nekoliko studija razvoja kontaktora masa usmjerenih na poboljšanje prijenosa tvari i energije u kontaktorima. Vezano uz prijenos tvari i topline, specificirano je da se kontakt između cirkulirajućih faza ostvaruje različitim tipovima kontaktora. Učinak prijenosa koreliran je s koeficijentom prijenosa tvari i topline s jedne strane te specifičnom površinom izmjene, tj. površinom izmjene po jedinici volumena kontaktora, s druge strane. Kontaktori se razlikuju po načinu kontakta faza (mjehurići, raspršenje, padajući film, itd.). Dok koeficijent izmjene ovisi o hidrodinamičkom režimu u kontaktoru (režim protoka i fizikalno-kemijska svojstva faza), specifična površina izmjene ovisi o njegovu načinu rada. Ograničenje njegove uporabe na neku određenu primjenu (fizikalno-kemijske pojave poput kristalizacije) zahtijeva istraživanje i razvoj uređaja koji bi više bili prilagođeni spomenutoj primjeni. Štoviše, najčešće upotrebljavani kontaktori u kemijskom inženjerstvu su kolone s pliticama, kolone s punilima, kolone s padajućim filmovima, kolone za raspršivanje, itd.

S ciljem povećanja izmjena, istražit će se novi praškasti apsorber i to s obzirom na fizikalno-kemijska svojstva faza i njihove hidrodinamičke uvjete strujanja u koloni za raspršivanje. Stoga je provedeno istraživanje utjecaja radnih varijabli (promjera mlaznice, protoka fluida, koncentracije fluida, veličine kapljica, itd.) na ukupni koeficijent prijenosa tvari u plinovitoj fazi u apsorberu rashladnog uređaja. Nakon fiksiranja tlaka u apsorberu, prvi dio istraživanja omogućio je razvoj novih korelacija koje povezuju eksperimentalne $K_G \cdot a$ rezultate sa svim radnim varijablama ($\dot{L}$,$\dot{G}$, d_d, itd.). Drugi dio bio je posvećen simulaciji rada apsorpcijskog rashladnog uređaja uvođenjem koncepta energetskih i eksergijskih prinosa temeljenih na izrazima za prijenos tvari.

Ključne riječi

H_2O/LiBr binarni sustav, ravnoteža para-kapljevina, hidrodinamika apsorbera s raspršivanjem, ukupni koeficijent prijenosa tvari, modeliranje

[a] *Processes Engineering Department, University of Hassiba Benbouali Chlef, Green Chemistry-Water-Energy Laboratory, B.P. 151, Chlef 02 000, Alžir*
[b] *Processes Engineering Department, Water and Environment Laboratory, University of Hassiba Benbouali, B.P. 151, Chlef 02 000, Alžir*
[c] *Department of Environmental Engineering, Eskisehir Technical University, 26 555 Eskisehir, Turska*
[d] *Engineering Faculty, Life Science and Biomedical Engineering Application and Research Center, Istanbul Gelisim University, 34 310 Istanbul, Turska*

Izvorni znanstveni rad
Prispjelo 13. studenoga 2021.
Prihvaćeno 17. ožujka 2022.